




Research Article

A Broadband Green-Red Vegetation Index for Monitoring Gross Primary Production Phenology

Gaofei Yin ^{1,2,3} Alexandre Verger ^{2,3,4} Adrià Descals^{2,3} Iolanda Filella^{2,3}
and Josep Peñuelas ^{2,3}

¹Faculty of Geosciences and Environmental Engineering, Southwest Jiaotong University, Chengdu 610031, China

²CREAF, Cerdanyola del Vallès, 08193 Catalonia, Spain

³CSIC, Global Ecology Unit CREAM-CSIC-UAB, Bellaterra 08193 Catalonia, Spain

⁴Desertification Research Centre CIDE-CSIC, València 46113, Spain

Correspondence should be addressed to Gaofei Yin; coffing@163.com

Received 23 June 2021; Accepted 16 February 2022; Published 19 March 2022

Copyright © 2022 Gaofei Yin et al. Exclusive Licensee Aerospace Information Research Institute, Chinese Academy of Sciences. Distributed under a Creative Commons Attribution License (CC BY 4.0).

The chlorophyll/carotenoid index (CCI) is increasingly used for remotely tracking the phenology of photosynthesis. However, CCI is restricted to few satellites incorporating the 531 nm band. This study reveals that the Moderate Resolution Imaging Spectroradiometer (MODIS) broadband green reflectance (band 4) is significantly correlated with this xanthophyll-sensitive narrowband (band 11) ($R^2 = 0.98, p < 0.001$), and consequently, the broadband green-red vegetation index GRVI—computed with MODIS band 1 and band 4—is significantly correlated with CCI—computed with MODIS band 1 and band 11 ($R^2 = 0.97, p < 0.001$). GRVI and CCI performed similarly in extracting phenological metrics of the dates of the start and end of the season (EOS) when evaluated with gross primary production (GPP) measurements from eddy covariance towers. For EOS extraction of evergreen needleleaf forest, GRVI even overperformed solar-induced chlorophyll fluorescence which is seen as a direct proxy of plant photosynthesis. This study opens the door for GPP and photosynthetic phenology monitoring from a wide set of sensors with broadbands in the green and red spectral regions.

1. Introduction

Terrestrial gross primary production (GPP), the total amount of carbon dioxide (CO_2) assimilated by plants by photosynthesis, is the most variable and uncertain flux in the global carbon cycle [1]. Accurate characterization of the spatiotemporal dynamics of GPP is crucial for improving our understanding of the responses and feedbacks of vegetation to climate change.

Remote sensing provides a feasible way to track GPP dynamics at a large scale, but it is still not straightforward to achieve spatiotemporally continuous monitoring with high reliability [1]. The recently emerging satellite-recorded solar-induced chlorophyll fluorescence (SIF) opened a new avenue to directly track GPP, considering its mechanistical link with plant photosynthesis [2]. However, the temporal frequency and spatial resolution of current SIF satellite products are still very limited [3, 4]. Therefore, primary productivity models based on simple light-use efficiency (LUE)

considerations still prevail in GPP community. Primary productivity models represent GPP as the product of absorbed photosynthetically active radiation (APAR) and LUE [5]. This LUE paradigm provides a robust and simple framework for calculating GPP from satellite observations [6]. APAR is closely related with the normalized difference vegetation index (NDVI), a measure of vegetation green biomass [7]. The key to estimating GPP using an LUE model is the determination of LUE. LUE is commonly parameterized by identifying the maximum LUE for each biome and then downregulating based on stress conditions, expressed using climatic variables, e.g., vapor-pressure deficit, temperature, and soil-moisture concentration [8, 9]. This parameterization involves meteorological data and preassigned maximum LUE, which are both uncertainty-prone. Therefore, LUE parameterization is one of the main sources of uncertainty in estimates of GPP [6, 10, 11].

The photochemical reflectance index (PRI) provides a promising way to determine LUE directly from satellite

measurements [12]. The underlying mechanisms of PRI for representing LUE vary with the timescale: PRI represents both the diurnal activity of the xanthophyll cycle and seasonal changes in chlorophyll/carotenoid pigment ratios [13].

PRI was originally calculated as the normalized difference between reflectances at 531 and 570 nm, serving as xanthophyll-sensitive and reference bands, respectively [14–16]. There are very few satellite-based sensors equipped with these two spectral bands simultaneously. For example, MODIS, the mostly used sensor for calculating satellite-PRI, only has the xanthophyll-sensitive band (band 11, 526–536 nm). Many alternative bands were therefore adopted as the reference band, e.g., bands 1 (620–670 nm), 4 (545–565 nm), 10 (483–493 nm), 12 (546–556 nm), and 13 (662–672 nm) [11, 17–19], resulting in different “MODIS PRI” indices. Recent studies have demonstrated that the “MODIS PRI” calculated using bands 1 and 11 is closely linked to the seasonal changes in chlorophyll/carotenoid pigments and was therefore renamed as the chlorophyll/carotenoid index (CCI) [7, 20]. CCI has been widely used to track GPP dynamics [20–24]. Especially, CCI was found suitable to timely capture the photosynthesis downregulation around the end of growing season, improving the accuracy of traditional broadband red and near-infrared vegetation indices such as NDVI for photosynthetic phenology estimation [25, 26].

Although CCI provides a reliable tool to monitor GPP dynamics, it can be calculated from a very few sensors (e.g., MODIS), because most of the current running optical satellites lack the xanthophyll-sensitive narrowband. In addition, chlorophyll/carotenoid ratio retrieval is very challenging because of the high atmospheric contamination [27]. Many studies revealed atmospheric correction would not improve and even reduce the performance of CCI [17, 18, 28, 29]. We hypothesized that the xanthophyll-sensitive narrowband MODIS band 11 (ranging from 526 to 536 nm) and the broadband in the green and MODIS band 4 (ranging from 545 to 565 nm) are highly correlated. If this hypothesis holds, the applicability of CCI would substantially improve, considering the ready availability of broadband green reflectances from existing multispectral sensors.

In fact, the normalized difference between broadband green and red reflectances has long been proposed [30] and was later named as green-red vegetation index (GRVI) [31]. However, its potential in capturing GPP dynamics may be underevaluated. GRVI has been reported to outperform the commonly used NDVI and enhanced vegetation index (EVI) in tracking plant photosynthesis [32, 33].

This study is aimed at evaluating the validity of GRVI, as an alternative to CCI, for monitoring gross primary production and vegetation phenology. Specific scientific questions include the following: (1) whether the MODIS-derived GRVI and CCI highly correlate with each other and (2) how well does GRVI track the dynamics of GPP, especially for the end of season when a temporal lag between NDVI and GPP often occurs.

2. Materials and Methods

2.1. Vegetation Indices. CCI can be calculated from MODIS reflectance data as

$$CCI = \frac{B_{11} - B_1}{B_{11} + B_1}, \quad (1)$$

where B_1 and B_{11} are the surface reflectances in MODIS band 1 (620–670 nm) and band 11 (526–536 nm), respectively.

The underlying spectroscopic mechanism of CCI is the foliar spectra in the green-red region, which is mainly controlled by pigmentation (Figure 1). The reflectance for summer acclimated leaves is much higher at the green than the red band. Winter acclimated leaves, which often have a lower chlorophyll/carotenoid pigment ratio [34], are characterized by higher reflectance except around 531 nm (MODIS band 11), leading to lower CCI values (Equation (1)). CCI is therefore a reliable indicator of the temporal variation of the chlorophyll/carotenoid pigment ratio, which indicates photosynthetic downregulation during autumn and winter [7, 20, 21, 24, 26].

GRVI was established based on the contrasting reflectances at green and red bands. GRVI can be calculated from MODIS band 1 (B_1) and band 4 (545–565 nm) (B_4), as

$$GRVI = \frac{B_4 - B_1}{B_4 + B_1}. \quad (2)$$

Although the GRVI and CCI are mechanistically different, they may be similar at satellite scale because the reflectance change caused by varied chlorophyll/carotenoid pigment ratio is quite subtle, compared with other confounding factors, e.g., atmospheric disturbance [27]. Therefore, we inferred that bands 4 and 11 may exhibit high consistence, considering their close spectral distance.

For comparison, the commonly used NDVI and the EVI, as well as the solar-induced chlorophyll fluorescence (SIF), were also employed in this study. NDVI and EVI were calculated from the MODIS reflectance data in bands B_1 (620–670 nm), B_2 (841–8756 nm), and B_3 (459–479 nm), as

$$\begin{aligned} NDVI &= \frac{B_2 - B_1}{B_2 + B_1}, \\ EVI &= 2.5 \frac{B_2 - B_1}{B_2 + 6B_1 - 7.5B_3 + 1}. \end{aligned} \quad (3)$$

SIF was extracted from GOSIF dataset with a resolution of 0.05° and 8 days. GOSIF used a machine learning method to predict Orbiting Carbon Observatory-2 observations with MODIS EVI and meteorological data (specifically, photosynthetically active radiation, vapor pressure deficit, and air temperature) as explanatory variables [35].

2.2. Data. *In situ* GPP time series from the FLUXNET-2015 dataset [36] were used as a benchmark to assess the performance of GRVI in tracking GPP dynamics. Daily GPP calculated from a nighttime method [37] was used. We selected

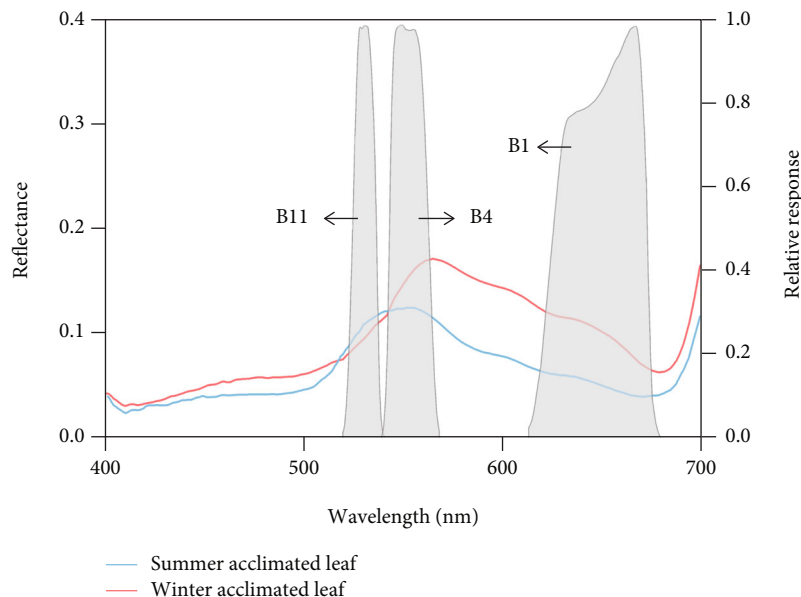


FIGURE 1: Spectra of typical summer and winter acclimated leaves. The shaded areas denote the spectral response functions of MODIS bands 1 (B1), 4 (B4), and 11 (B11). The spectra were for *Pinus contorta* (lodgepole pine) seedlings edited from Gamon et al. [7].

27 grasslands, 37 evergreen needleleaf forests, and 21 deciduous broadleaf forests. Detailed information for each site is presented in Table S1. Sites were selected based on the criteria: (1) they were in the Northern Hemisphere at latitudes $> 30^\circ$, and (2) they had at least three years of concomitant in situ GPP and MODIS observations for 2001-2020.

We used the daily MCD19A1 Version 6 [38] to calculate CCI, GRVI, NDVI, and EVI, for two main reasons: (1) it uses an adaptive time series and a spatial analysis, the Multi-Angle Implementation of Atmospheric Correction (MAIAC) algorithm, to derive atmospheric aerosol concentrations and surface reflectances without empirical assumptions to obtain a more accurate surface reflectance, and (2) reflectances at bands 1, 2, 3, 4, and 11 are all delivered, allowing the comparison between CCI, GRVI, NDVI, and EVI. All the bands were resampled to 1 km.

Data contaminated by clouds, snow, or a high aerosol optical depth were excluded. MCD19A1 data with viewing zenith angles $> 40^\circ$ were also excluded to minimize the anisotropic effects of the reflectance [19, 25].

2.3. Statistical Analysis. We firstly compared the reflectances at MODIS bands 11 and 4 and also compared the, respectively, derived CCI vs. GRVI over all the selected 115,916 reflectance samples.

We evaluated the performance of CCI, GRVI, NDVI, EVI, and SIF for tracking GPP and retrieving phenological metrics as compared to FLUXNET GPP. The maximum-separation (MS) method was adopted to extract the dates of the start of season (SOS) and end of season (EOS) [39]. MS is a variant of the threshold method and applies a moving window that estimates the ratio of observations that exceed a threshold (50%, in this study) before and after the central day. SOS/EOS is the day of the year when the difference between the ratios before and after the central day are

minimum/maximal. Details for MS are provided in our previous study [39]. SOS/EOS was estimated from CCI, GRVI, NDVI, EVI, SIF, and FLUXNET GPP. SOS and EOS from GPP were seen as the references of starting and ending days of photosynthetically active season, respectively. Note that, before phenology extraction, the daily vegetation indices and GPP were resampled to 8-day temporal resolution with a maximum-value composting method to smooth the noise in the time series.

3. Results

The reflectances from MODIS bands 4 and 11 were highly consistent ($R^2 = 0.98$), and the correlation was significant ($p < 0.001$) (Figure 2). This consistency was propagated to the derived vegetation indices: the GRVI could reproduce the CCI with a robust regression of $y = 0.98x - 0.074$ ($R^2 = 0.97, p < 0.001$); i.e., the GRVI, based on the green broadband, is a reliable proxy of CCI.

US-Oho, CA-TP3, and US-IB2, were selected as examples of deciduous broadleaf forest (DBF), evergreen needleleaf forest (ENF), and grassland (GRA), respectively, to illustrate the seasonal dynamics of GPP and the capacity of different vegetation indices to capture its dynamics (Figure 3). During spring season, GPP and all the vegetation indices increased rapidly and nearly at the same time, as reflected by the narrow range of variation of SOS values especially for grassland (Figure 3(c)). Contrarily, the decrease during the senescence process was gradual. The satellite vegetation indices showed a systematic positive temporal lag difference (i.e., a delay in phenology) compared to ground GPP measurements. NDVI showed the highest positive lag in autumn phenology compared with GPP, implying that photosynthesis shuts down even when plants still have high green biomass. CCI and GRVI were very similar

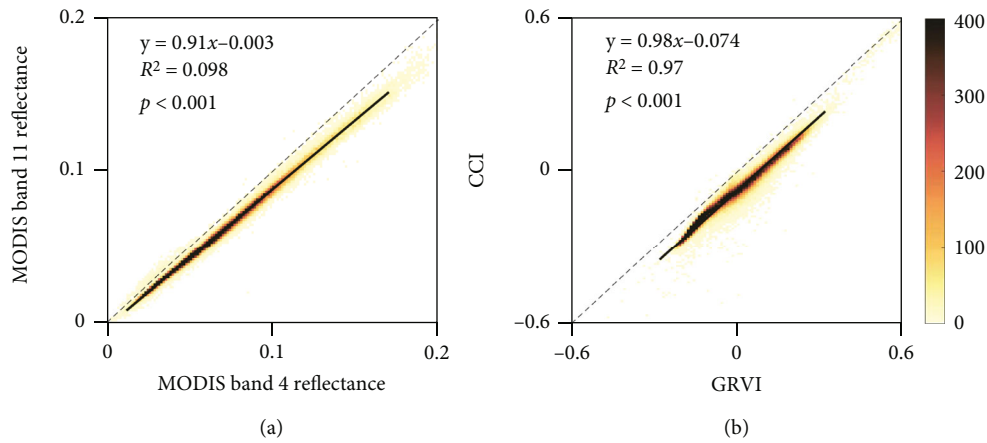


FIGURE 2: Density scatter plots of the reflectances from MODIS bands 4 and 11 (a) and of the broadband green-red vegetation index (GRVI) vs. the original narrowband chlorophyll/carotenoid index (CCI) (b).

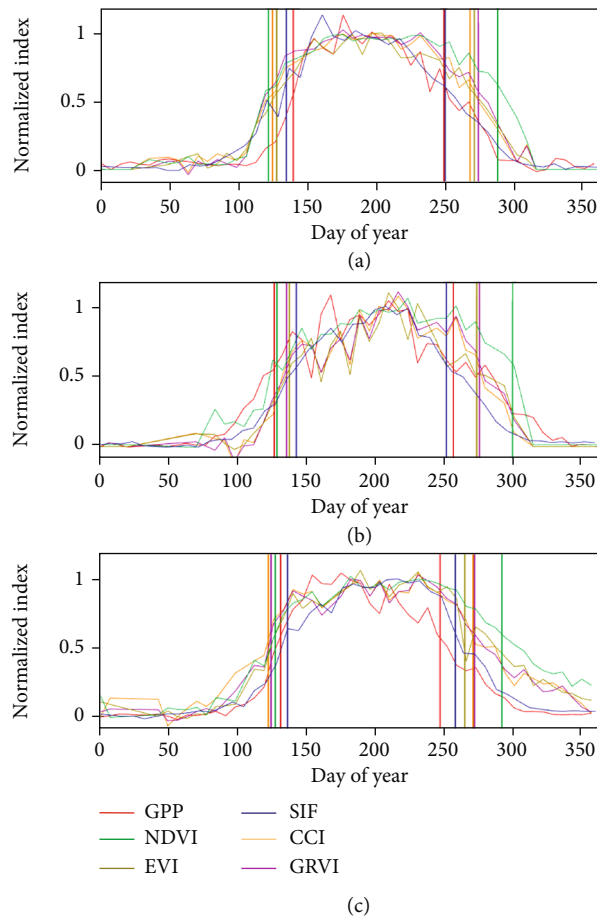


FIGURE 3: Temporal profiles of in situ gross primary production (GPP), normalized difference vegetation index (NDVI), enhanced vegetation index (EVI), solar-induced chlorophyll fluorescence (SIF), chlorophyll/carotenoid index (CCI), and green-red vegetation index (GRVI) for a deciduous broadleaf forest (a), an evergreen needleleaf forest (b), and a grassland (c). The vertical lines show the extracted phenology from a maximum-separation (MS) method. US-Oho (in 2006), CA-TP3 (in 2013), and US-IB2 (in 2011) were selected as examples of grassland, deciduous broadleaf forest, and evergreen needleleaf forest, respectively. For a better comparison, all the indices were linearly normalized to the range of [0, 1].

throughout the growing season, but GRVI lagged slightly compared with the CCI, especially for the forests (Figures 3(a) and 3(b)).

Compared with the GPP-derived SOS, those from the satellite indices all exhibit earlier estimates over DBF (Figure 4), with the largest and least bias happen for NDVI

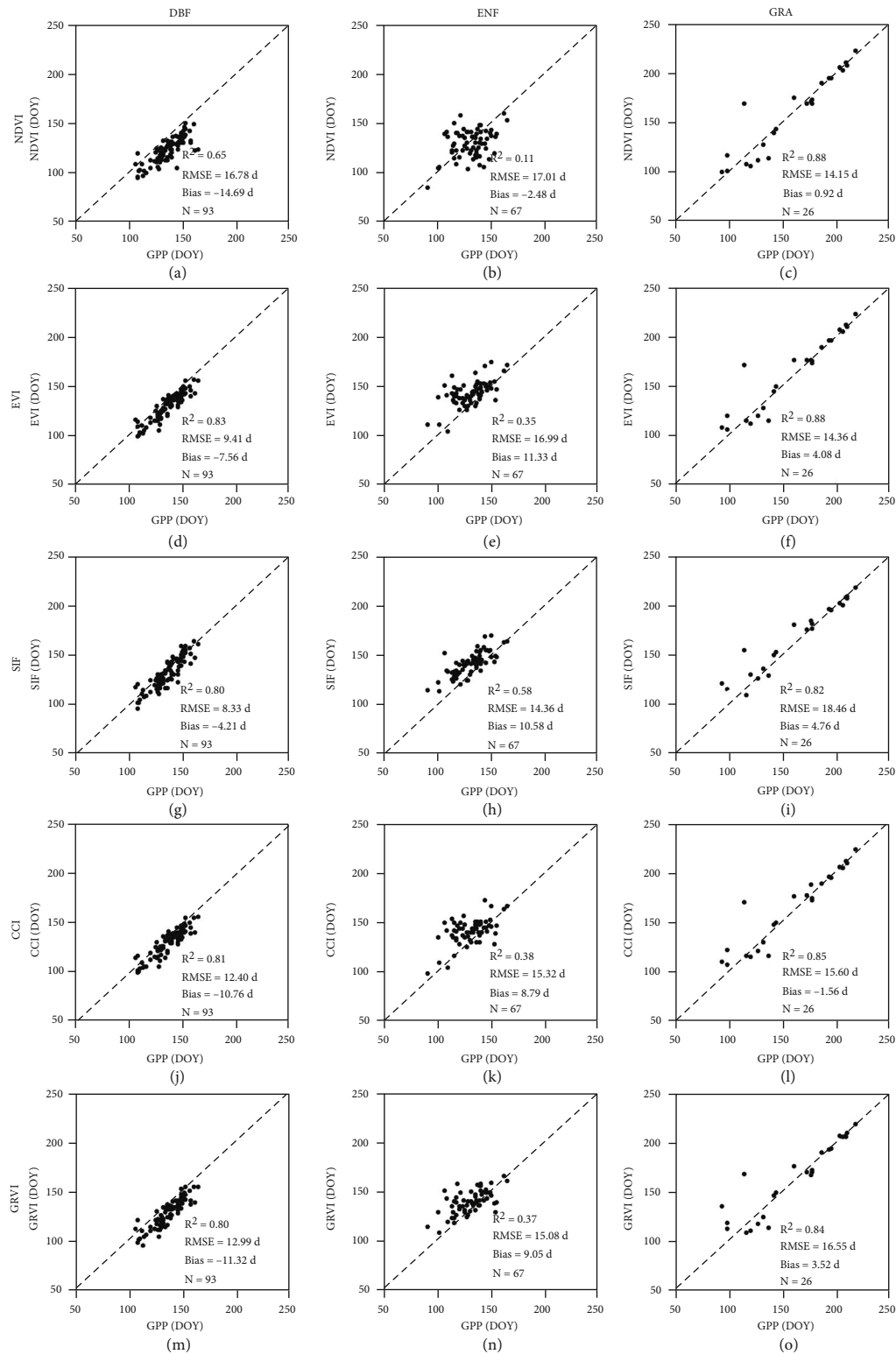


FIGURE 4: Scatterplots of the dates of the start of the season (SOS) estimated using the vegetation indices and in situ gross primary production (GPP) for deciduous broadleaf forest (DBF), evergreen needleleaf forest (ENF), and grassland (GRA). SOS dates were extracted using the Maximum Separation method [39]. The referred statistics are the correlation coefficient (R^2), the root mean square error (RMSE), and the mean bias. DOY: day of year.

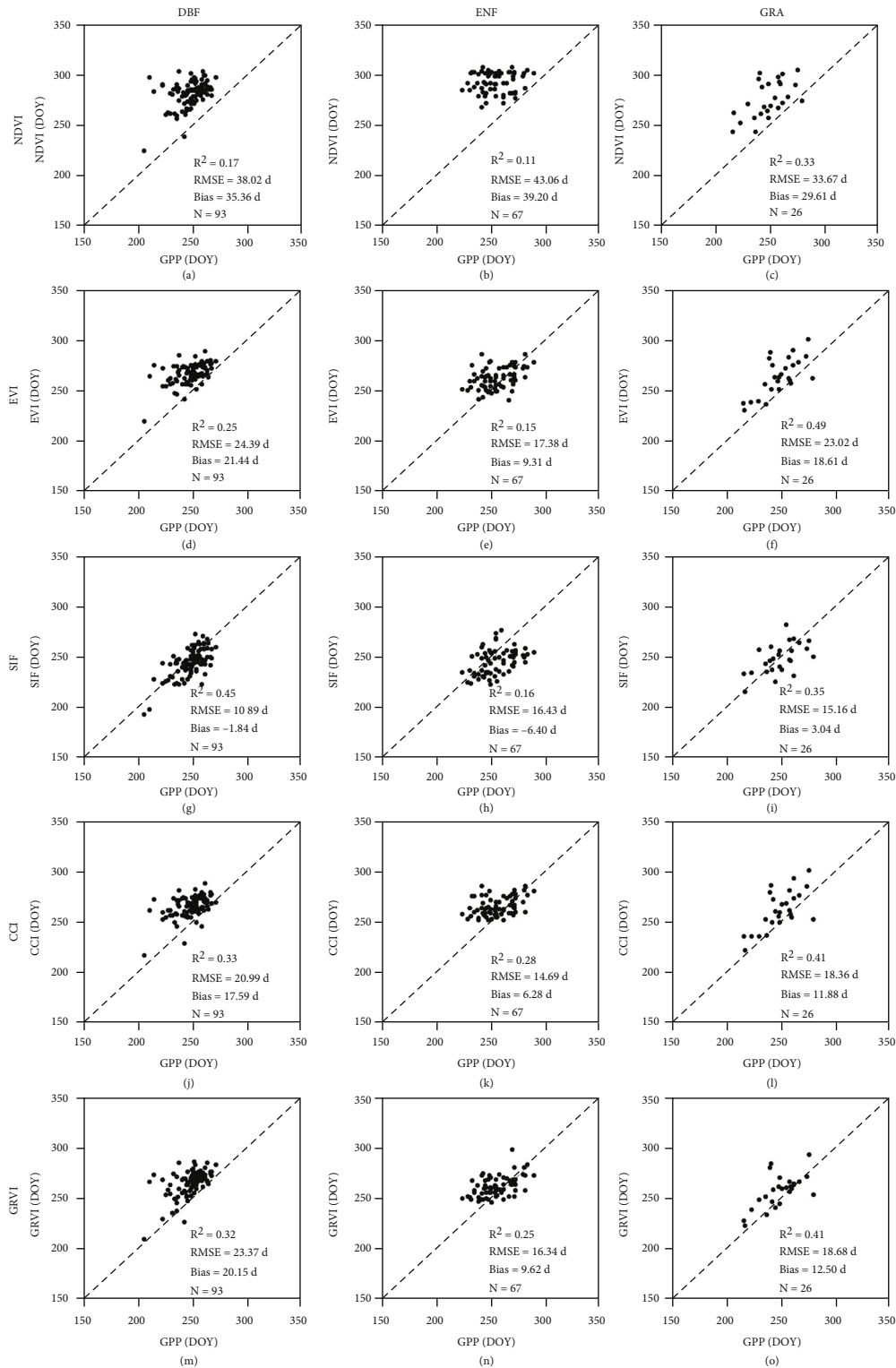


FIGURE 5: Scatterplots of the dates of the end of the season (EOS) estimated using the vegetation indices and in situ gross primary production (GPP) for deciduous broadleaf forest (DBF), evergreen needleleaf forest (ENF), and grassland (GRA). EOS dates were extracted using the Maximum Separation method [39]. The referred statistics are the correlation coefficient (R^2), the root mean square error (RMSE), and the mean bias. DOY: day of year.

(Figure 4(a)) and SIF (Figure 4(g)), respectively. Over the three selected vegetation types, SOS for ENF showed the highest uncertainty. For example, R^2 between NDVI and

GPP-derived SOS was 0.11. The best estimate was from SIF, with a R^2 of 0.58. For GRA, due to its simple structure, no obvious discrepancy was found for the SOS estimates

from the five indices. Generally, GRVI performed comparably with CCI in SOS estimation, and they both show similar performance as EVI. However, closer inspection reveals that GRVI and CCI both obtained better accuracy than EVI for ENF, for which CCI was originally designed [7, 20].

EOS dates estimated using NDVI were considerably delayed compared with the reference dates using GPP for all selected vegetation types (Figures 5(a)–5(c) for DBF, ENF, and GRA, respectively). The highest bias was observed in ENF sites (43.03 days) (Figure 5(b)). Compared with NDVI, the lag of the estimated EOS from other indices was remarkably mitigated; e.g., the bias for ENF was reduced to 6.28 and 9.63 d for CCI and GRVI, respectively. GRVI performed comparably than CCI over all site-years, with only slightly more delayed estimates: 2.56 (20.15–17.59), 3.35 (9.63–6.28), and 0.62 (12.5–11.88) d for DBF, ENF, and GRA, respectively. As expected, SIF performed very well for every vegetation type. Yet, CCI and GRVI showed slightly better performances, in terms of R^2 and RMSE, than SIF for EOS retrieval over ENF.

4. Discussion

This study demonstrated that at the satellite scale the MODIS narrowband CCI can be reproduced with the broadband GRVI. GRVI performed satisfactorily in tracking GPP dynamic over DBF, ENF, and GRA vegetation types.

The physiological chlorophyll/carotenoid index (CCI) was originally designed for ENF [7] but also well represents GPP variation for other vegetation types, e.g., DBF [23] and GRA [25]. The advantage of CCI to track GPP mainly lies in the extraction of the end of the photosynthetically active season (EOS) [26]. For deciduous plants (including DBF and GRA), senescence follows a physiological timetable: (1) reallocation of foliar nutrients, (2) degradation of chlorophyll, (3) foliar coloration, and (4) foliar abscission. The reallocation of foliar nutrients is difficult to detect with remote sensing but is strongly associated with the degradation of chlorophyll (with decreasing chlorophyll/carotenoid ratio) [40]. As for evergreen plants, the absorbed light during late autumn cannot be fully exploited for carbon uptake because of environmental stress (e.g., low temperature) [41]. Such an imbalance between light energy supply and utilization activates a mechanism which adjusts leaf pigment pools and dissipates excess energy by increasing the carotenoid/chlorophyll ratio [13, 42]. Therefore, CCI is more capable of capturing the downregulation of plant photosynthesis than other vegetation indices more sensitive to green biomass [26].

Previous studies revealed that NDVI was mainly determined by vegetation structure and EVI is relatively more controlled by leaf coloration [43]. This explains why the observed positive temporal lag phenomenon in EOS extraction was shorter for EVI (with less bias compared with GPP EOS) than for NDVI. Compared with NDVI and EVI, GRVI was capable of capturing the reflectance contrast between the green hump and red valley (see Figure 1) which are mainly determined by leaf chlorophyll content. Leaf chlorophyll content was found a good proxy of maximum photo-

synthetic rate ([44]). GRVI therefore performed better than NDVI and EVI to extract photosynthetic phenology, especially for EOS. SIF, a direct “proxy” of plant photosynthesis [2], was also employed as a reference to assess the performance of GRVI in GPP tracking. Our results reveal that GRVI derived from MODIS data performs comparably with SIF derived from GOSIF data. GOSIF has, however, a lower spatial resolution and revisit frequency (0.05° every 8-day temporal frequency) than MCD19A1 data (1 km spatial resolution and 1-day temporal frequency). The current existing SIF datasets are indeed characterized by low spatial resolution and temporal frequency, so the GRVI here defined provides a useful complementary or even alternative tool for high spatiotemporal GPP monitoring.

We found that MODIS bands 11 (narrow green band, sensitive to xanthophyll interconversion) and 4 (wide green band, signaling leaf chlorophyll content) were highly correlated at the seasonal scale (Figure 2(a)), so CCI (Equation (1)) can be safely reproduced by GRVI (Equation (2)). The direct comparison between CCI and GRVI (Figure 2(b)), the comparison with FLUXNET GPP, and the validation of phenology metrics supported our hypothesis of equivalence between CCI and GRVI for monitoring GPP and phenology. Considering that band 4 has higher spatial resolution (500 m) than band 11 (1 km), MODIS GRVI is capable of characterizing GPP seasonality at smaller granularity than CCI. Furthermore, the calculation of GRVI is easy to transfer to other sensors, because the green and red broadband are readily available on most existing multispectral sensors. Note that the xanthophyll-sensitive narrowband (~ 531 nm) was removed in the VIIRS, the successor of MODIS [45]. The application of MODIS CCI, however, can be continuously persisted by GRVI from VIIRS.

GRVI can quantify the maximum leaf photosynthetic rate ([32, 33]); therefore, performs satisfactory in tracking GPP dynamics, even for the evergreen forests [32, 33, 46]. Other indices were also reported having the potential to capture the pigment variation and deserved further assessment. For example, Penuelas et al. [16] found that the red and blue bands were the best combination to capture the variation of chlorophyll/carotenoid pigment ratios (Normalized Difference Pigment Index (NDPI) = (red-blue)/(red + blue) and Structural Independent Pigment Index (SIPI) = (IR-blue)/(IR-red)). The blue band, however, was highly sensitive to atmospheric distortion, so the feasibility of NDPI or SIPI calculated from satellite observations remains unknown. Red edge bands were also found highly sensitive to pigment content, especially to chlorophyll content [47]. Therefore, red edge-based vegetation indices, e.g., MERIS Terrestrial Chlorophyll Index (MTCI) and OLCI Terrestrial Chlorophyll Index (OTCI) [48], were also worth assessment in terms of photosynthetic phenology extraction.

This study demonstrated that MODIS CCI could be reproduced by the GRVI. GRVI can be directly transferred to other satellites considering the readily availability of broadband green and red bands. We will assess the application of GRVI to Landsat 8, Sentinel-2, and other commonly used optical satellites in future studies. Future studies should

focus on assessing the feasibility of GRVI to retrieve chlorophyll/carotenoid ratio also as compared with MODIS CCI and ground data. Residual atmospheric contamination effects on CCI also require further attention [27]. Finally, we will also test other band combinations and investigate red-edge and blue bands from Sentinel-2 and Sentinel-3 in a future study.

5. Conclusions

This study demonstrated that MODIS-derived CCI, originally calculated with the support of the narrow xanthophyll-sensitive (~531 nm) band, could be safely reproduced by wide green and red bands, GRVI ($R^2 = 0.97$), for monitoring GPP and phenology. The comparison with FLUXNET GPP showed that the broadband GRVI performed comparably with the original CCI in tracking the dynamics of GPP and for extracting the dates of the start and end of the photosynthetically active season. GRVI provides a powerful and robust tool for monitoring the temporal variation of photosynthesis activity from a wide set of sensors with broadbands in the green and red spectral regions.

Data Availability

The data that support the findings of this study are available from the corresponding author upon request.

Conflicts of Interest

The authors declare that there is no conflict of interest regarding the publication of this article.

Authors' Contributions

G.Y. did the conceptualization. G.Y. is responsible for the writing—original draft. A.V., A.D., I.F., and J.P. is assigned to the writing—review and editing.

Acknowledgments

This work was supported by the Sichuan Science and Technology Program (2021JDJQ0007 and 2020JDTD0003), the National Natural Science Foundation of China (41971282), and the Marie Skłodowska-Curie Grant of the European Union's Horizon 2020 Research and Innovation Programme (835541). Funding from the Spanish Government (grant PID2019-110521GB-I00), Fundación Ramon Areces (grant ELEMENTAL-CLIMATE), Catalan Government (grants SGR 2017-1005 and AGAUR-2020PANDE00117), and European Research Council (Synergy grant ERC-SyG-2013-610028, IMBALANCE-P) is also acknowledged. This work represents a contribution to CSIC-PTI TELEDETECT. *In situ* observations of fluxes were obtained from the FLUXNET 2015 dataset (<http://fluxnet.fluxdata.org/data/fluxnet2015-dataset/>). The MCD19A1 C6 product is also available online (<https://ladsweb.modaps.eosdis.nasa.gov/search/>). Jiangliu Xie, Hongfan Gu, and Huiqin Pan are appreciated for collecting the data.

Supplementary Materials

Table S1: description of the FLUXNET sites. DBF: deciduous broadleaf forest; ENF: evergreen needleleaf forest; GRA: grassland. (*Supplementary Materials*)

References

- [1] A. Anav, P. Friedlingstein, C. Beer et al., "Spatiotemporal patterns of terrestrial gross primary production: a review," *Reviews of Geophysics*, vol. 53, no. 3, pp. 785–818, 2015.
- [2] A. Porcar-Castell, E. Tyystjarvi, J. Atherton et al., "Linking chlorophyll a fluorescence to photosynthesis for remote sensing applications: mechanisms and challenges," *Journal of Experimental Botany*, vol. 65, no. 15, pp. 4065–4095, 2014.
- [3] C. Frankenberg, J. B. Fisher, J. Worden et al., "New global observations of the terrestrial carbon cycle from GOSAT: patterns of plant fluorescence with gross primary productivity," *Geophysical Research Letters*, vol. 38, no. 17, 2011.
- [4] L. Guanter, C. Bacour, A. Schneider et al., "The TROPISIF global sun-induced fluorescence dataset from the Sentinel-5P TROPOMI mission," *Earth System Science Data*, vol. 13, no. 11, pp. 5423–5440, 2021.
- [5] J. L. Monteith, "Solar radiation and productivity in tropical ecosystems," *Journal of Applied Ecology*, vol. 9, no. 3, pp. 747–766, 1972.
- [6] W. P. Yuan, S. Liu, G. S. Zhou et al., "Deriving a light use efficiency model from eddy covariance flux data for predicting daily gross primary production across biomes," *Agricultural and Forest Meteorology*, vol. 143, no. 3–4, pp. 189–207, 2007.
- [7] J. A. Gamon, K. F. Huemmrich, C. Y. Wong et al., "A remotely sensed pigment index reveals photosynthetic phenology in evergreen conifers," *Proceedings of the National Academy of Sciences of the United States of America*, vol. 113, no. 46, pp. 13087–13092, 2016.
- [8] S. W. Running, R. R. Nemani, F. A. Heinsch, M. S. Zhao, M. Reeves, and H. Hashimoto, "A continuous satellite-derived measure of global terrestrial primary production," *Bio-science*, vol. 54, no. 6, pp. 547–560, 2004.
- [9] B. D. Stocker, J. Zscheischler, T. F. Keenan, I. C. Prentice, S. I. Seneviratne, and J. Penuelas, "Drought impacts on terrestrial primary production underestimated by satellite monitoring," *Nature Geoscience*, vol. 12, no. 4, pp. 264–270, 2019.
- [10] C. Y. Wu, J. M. Chen, A. R. Desai et al., "Remote sensing of canopy light use efficiency in temperate and boreal forests of North America using MODIS imagery," *Remote Sensing of Environment*, vol. 118, pp. 60–72, 2012.
- [11] F. M. Zhang, J. M. Chen, J. Q. Chen, C. M. Gough, T. A. Martin, and D. Dragoni, "Evaluating spatial and temporal patterns of MODIS GPP over the conterminous U.S. against flux measurements and a process model," *Remote Sensing of Environment*, vol. 124, pp. 717–729, 2012.
- [12] J. Penuelas, M. F. Garbulsky, and I. Filella, "Photochemical reflectance index (PRI) and remote sensing of plant CO₂ uptake," *New Phytologist*, vol. 191, no. 3, pp. 596–599, 2011.
- [13] C. Y. Wong and J. A. Gamon, "Three causes of variation in the photochemical reflectance index (PRI) in evergreen conifers," *The New Phytologist*, vol. 206, no. 1, pp. 187–195, 2015.
- [14] J. A. Gamon, J. Penuelas, and C. B. Field, "A narrow-waveband spectral index that tracks diurnal changes in photosynthetic

- efficiency,” *Remote Sensing of Environment*, vol. 41, no. 1, pp. 35–44, 1992.
- [15] J. Penuelas, I. Filella, and J. A. Gamon, “Assessment of photosynthetic radiation-use efficiency with spectral reflectance,” *New Phytologist*, vol. 131, no. 3, pp. 291–296, 1995.
- [16] J. Penuelas, J. A. Gamon, A. L. Fredeen, J. Merino, and C. B. Field, “Reflectance indices associated with physiological changes in nitrogen- and water-limited sunflower leaves,” *Remote Sensing of Environment*, vol. 48, no. 2, pp. 135–146, 1994.
- [17] A. Goerner, M. Reichstein, E. Tomelleri et al., “Remote sensing of ecosystem light use efficiency with MODIS-based PRI,” *Biogeosciences*, vol. 8, no. 1, pp. 189–202, 2011.
- [18] M. He, J. S. Kimball, S. Running, A. Ballantyne, K. Guan, and F. Huemmrich, “Satellite detection of soil moisture related water stress impacts on ecosystem productivity using the MODIS-based photochemical reflectance index,” *Remote Sensing of Environment*, vol. 186, pp. 173–183, 2016.
- [19] E. M. Middleton, K. F. Huemmrich, D. R. Landis, T. A. Black, A. G. Barr, and J. H. McCaughey, “Photosynthetic efficiency of northern forest ecosystems using a MODIS-derived Photochemical Reflectance Index (PRI),” *Remote Sensing of Environment*, vol. 187, pp. 345–366, 2016.
- [20] C. Y. S. Wong, P. D’Odorico, M. A. Arain, and I. Ensminger, “Tracking the phenology of photosynthesis using carotenoid-sensitive and near-infrared reflectance vegetation indices in a temperate evergreen and mixed deciduous forest,” *The New Phytologist*, vol. 226, no. 6, pp. 1682–1695, 2020.
- [21] P. D’Odorico, A. Besik, C. Y. S. Wong, N. Isabel, and I. Ensminger, “High-throughput drone-based remote sensing reliably tracks phenology in thousands of conifer seedlings,” *The New Phytologist*, vol. 226, no. 6, pp. 1667–1681, 2020.
- [22] E. Frechette, C. Y. Chang, and I. Ensminger, “Variation in the phenology of photosynthesis among eastern white pine provenances in response to warming,” *Global Change Biology*, vol. 26, no. 9, pp. 5217–5234, 2020.
- [23] K. Springer, R. Wang, and J. Gamon, “Parallel seasonal patterns of photosynthesis, fluorescence, and reflectance indices in boreal trees,” *Remote Sensing*, vol. 9, no. 7, p. 691, 2017.
- [24] C. Y. S. Wong, P. D’Odorico, Y. Bhatena, M. A. Arain, and I. Ensminger, “Carotenoid based vegetation indices for accurate monitoring of the phenology of photosynthesis at the leaf-scale in deciduous and evergreen trees,” *Remote Sensing of Environment*, vol. 233, p. 111407, 2019.
- [25] R. Wang, J. A. Gamon, C. A. Emmerton, K. R. Springer, R. Yu, and G. Hmimina, “Detecting intra- and inter-annual variability in gross primary productivity of a North American grassland using MODIS MAIAC data,” *Agricultural and Forest Meteorology*, vol. 281, p. 107859, 2020.
- [26] G. Yin, A. Verger, I. Filella, A. Descals, and J. Peñuelas, “Divergent estimates of forest photosynthetic phenology using structural and physiological vegetation indices,” *Geophysical Research Letters*, vol. 47, no. 18, 2020.
- [27] N. Sabater, P. Kolmonen, S. Van Wittenberghe, A. Arola, and J. Moreno, “Challenges in the atmospheric characterization for the retrieval of spectrally resolved fluorescence and PRI region dynamics from space,” *Remote Sensing of Environment*, vol. 254, p. 112226, 2021.
- [28] G. G. Drolet, K. F. Huemmrich, F. G. Hall et al., “A MODIS-derived photochemical reflectance index to detect inter-annual variations in the photosynthetic light-use efficiency of a boreal deciduous forest,” *Remote Sensing of Environment*, vol. 98, no. 2-3, pp. 212–224, 2005.
- [29] A. Moreno, F. Maselli, M. A. Gilabert, M. Chiesi, B. Martínez, and G. Seufert, “Assessment of MODIS imagery to track light-use efficiency in a water-limited Mediterranean pine forest,” *Remote Sensing of Environment*, vol. 123, pp. 359–367, 2012.
- [30] C. J. Tucker, “Red and photographic infrared linear combinations for monitoring vegetation,” *Remote Sensing of Environment*, vol. 8, no. 2, pp. 127–150, 1979.
- [31] T. Motohka, K. N. Nasahara, H. Oguma, and S. Tsuchida, “Applicability of green-red vegetation index for remote sensing of vegetation phenology,” *Remote Sensing*, vol. 2, no. 10, pp. 2369–2387, 2010.
- [32] S. Nagai, T. Inoue, T. Ohtsuka et al., “Relationship between spatio-temporal characteristics of leaf-fall phenology and seasonal variations in near surface- and satellite-observed vegetation indices in a cool-temperate deciduous broad-leaved forest in Japan,” *International Journal of Remote Sensing*, vol. 35, no. 10, pp. 3520–3536, 2014.
- [33] S. Nagai, T. M. Saitoh, H. Kobayashi et al., “In situ examination of the relationship between various vegetation indices and canopy phenology in an evergreen coniferous forest, Japan,” *International Journal of Remote Sensing*, vol. 33, no. 19, pp. 6202–6214, 2012.
- [34] J. Penuelas, F. Baret, and I. Filella, “Semi-empirical indices to assess carotenoids chlorophyll-a ratio from leaf spectral reflectance,” *Photosynthetica*, vol. 31, pp. 221–230, 1995.
- [35] X. Li and J. F. Xiao, “Mapping Photosynthesis Solely from solar-induced chlorophyll Fluorescence: A Global, Fine-Resolution Dataset of Gross Primary Production derived from OCO-2,” *Remote Sensing*, vol. 11, no. 21, p. 2563, 2019.
- [36] G. Pastorello, C. Trotta, E. Canfora et al., “The FLUXNET2015 dataset and the ONEFlux processing pipeline for eddy covariance data,” *Sci Data*, vol. 7, no. 1, p. 225, 2020.
- [37] M. Reichstein, E. Falge, D. Baldocchi et al., “On the separation of net ecosystem exchange into assimilation and ecosystem respiration: review and improved algorithm,” *Global Change Biology*, vol. 11, no. 9, pp. 1424–1439, 2005.
- [38] A. I. Lyapustin, Y. Wang, I. Laszlo et al., “Multi-angle implementation of atmospheric correction for MODIS (MAIAC): 3. Atmospheric correction,” *Remote Sensing of Environment*, vol. 127, pp. 385–393, 2012.
- [39] A. Descals, A. Verger, G. Yin, and J. Penuelas, “A threshold method for robust and fast estimation of land-surface phenology using Google Earth Engine,” *IEEE Journal of Selected Topics in Applied Earth Observations and Remote Sensing*, vol. 14, 2021.
- [40] Y. Fracheboud, V. Luquez, L. Bjorken, A. Sjodin, H. Tuominen, and S. Jansson, “The control of autumn senescence in European Aspen,” *Plant Physiology*, vol. 149, no. 4, pp. 1982–1991, 2009.
- [41] G. Oquist and N. P. Huner, “Photosynthesis of overwintering evergreen plants,” *Annual Review of Plant Biology*, vol. 54, no. 1, pp. 329–355, 2003.
- [42] J. Kim, Y. Ryu, B. Dechant et al., “Solar-induced chlorophyll fluorescence is non-linearly related to canopy photosynthesis in a temperate evergreen needleleaf forest during the fall transition,” *Remote Sensing of Environment*, vol. 258, p. 112362, 2021.
- [43] X. M. Xiao, D. Hollinger, J. Aber et al., “Satellite-based modeling of gross primary production in an evergreen needleleaf

- forest," *Remote Sensing of Environment*, vol. 89, no. 4, pp. 519–534, 2004.
- [44] H. Croft, J. M. Chen, X. Z. Luo, P. Bartlett, B. Chen, and R. M. Staebler, "Leaf chlorophyll content as a proxy for leaf photosynthetic capacity," *Global Change Biology*, vol. 23, no. 9, pp. 3513–3524, 2017.
- [45] D. Hillger, T. Kopp, T. Lee et al., "First-light imagery from Suomi NPP VIIRS," *Bulletin of the American Meteorological Society*, vol. 94, no. 7, pp. 1019–1029, 2013.
- [46] A. A. Gitelson, Y. J. Kaufman, R. Stark, and D. Rundquist, "Novel algorithms for remote estimation of vegetation fraction," *Remote Sensing of Environment*, vol. 80, no. 1, pp. 76–87, 2002.
- [47] I. Filella and J. Penuelas, "The red edge position and shape as indicators of plant chlorophyll content, biomass and hydric status," *International Journal of Remote Sensing*, vol. 15, no. 7, pp. 1459–1470, 1994.
- [48] J. Clevers and A. A. Gitelson, "Remote estimation of crop and grass chlorophyll and nitrogen content using red-edge bands on Sentinel-2 and -3," *International Journal of Applied Earth Observation and Geoinformation*, vol. 23, pp. 344–351, 2013.